

One-Step Diffusion Transformer for Controllable Real-World Image Super-Resolution

Yushun Fang^{1,2,*} Yuxiang Chen^{2,*} Shibo Yin^{2,†} Qiang Hu^{1,†} Jiangchao Yao¹
 Ya Zhang¹ Xiaoyun Zhang^{1,†} Yanfeng Wang¹
¹Shanghai Jiao Tong University ²Xiaohongshu Inc
 *Equal contribution [†]Corresponding author

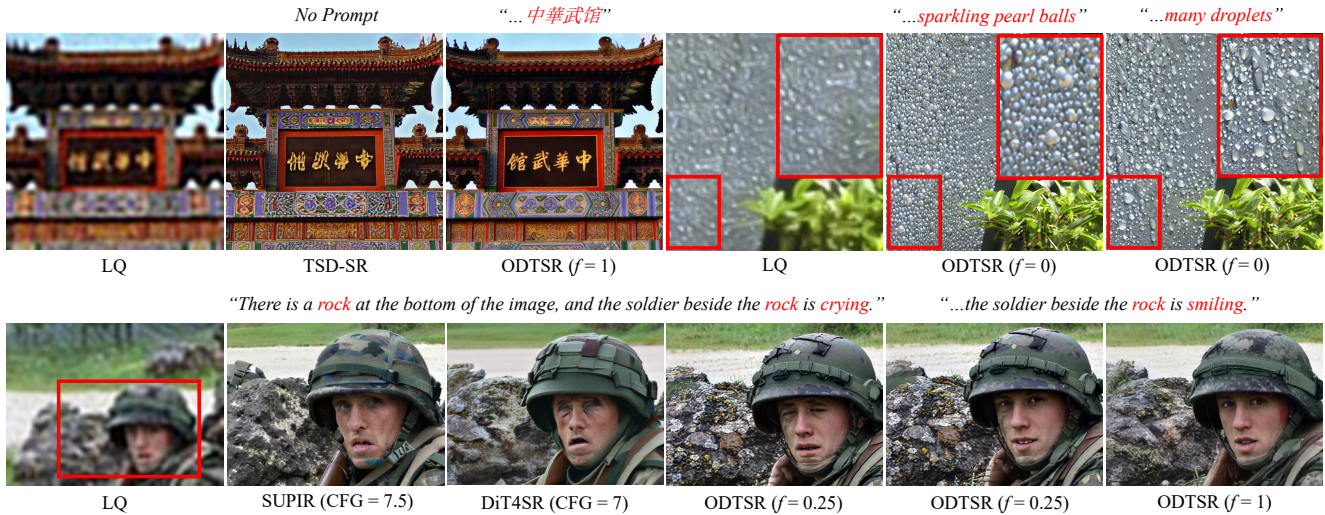


Figure 1. **Controllable Real-ISR:** Qualitative results of our ODTSR and other state-of-the-art methods. Our method achieves superior quality, supports flexible bilingual prompt controllability, and covers challenging sub-domains such as Chinese text images, fine-grained texture and face images. “ f ” denotes controllable *Fidelity Weight* in ODTSR. More results are shown in the **supplementary materials**.

Abstract

Recent advances in diffusion-based real-world image super-resolution (Real-ISR) have demonstrated remarkable perceptual quality, yet the balance between fidelity and controllability remains a problem: multi-step diffusion-based methods suffer from generative diversity and randomness, resulting in low fidelity, while one-step methods lose control flexibility due to fidelity-specific finetuning. In this paper, we present **ODTSR**, a one-step diffusion transformer based on *Qwen-Image* that performs Real-ISR considering fidelity and controllability simultaneously: a newly introduced visual stream receives low-quality images (LQ) with adjustable noise (Control Noise), and the original visual stream receives LQs with consistent noise (Prior Noise), forming the Noise-hybrid Visual Stream (NVS) design. ODTSR further employs Fidelity-aware Adversarial Training (FAA) to enhance controllability and achieve one-step inference. Extensive experiments demonstrate that ODTSR not only achieves state-of-the-art (SOTA) perfor-

mance on generic Real-ISR, but also enables prompt controllability on challenging scenarios such as real-world scene text image super-resolution (STISR) of Chinese characters without training on specific datasets.

1. Introduction

Real-ISR[35] aims to restore real-world low-quality, low-resolution images (LQ) to corresponding high-quality, high-resolution images (HR). Fidelity is fundamental for Real-ISR, however, under conditions of complex degradation and ambiguous semantics of LQ, the restoration of HR is not unique, which constitutes a classic ill-posed problem, inherently leading to demands on controllability.

In recent years, diffusion models have achieved remarkable perceptual quality in Real-ISR. However, simultaneously ensuring fidelity and controllability remains a challenge in the field. Multi-step diffusion approaches possess powerful generative controllability through iterative denois-

Table 1. **Overall Comparison.** We compare four SOTA methods with our proposed ODTSR. ODTSR achieves fidelity and prompt controllability simultaneously while achieving one-step inference. “✓✓” denotes ODTSR support both English and Chinese prompts.

Method	One step	Fidelity	Prompt Control
PiSA-SR	✓	✓	✗
TSD-SR	✓	✓	✗
SUPIR	✗	✗	✓
DiT4SR	✗	✓	✓
ODTSR (Ours)	✓	✓	✓✓

ing, but tend to suffer from randomness, resulting in divergence from LQ, as well as expensive inference time. In contrast, one-step methods offer efficiency advantages, yet often lose the inherent controllability of pretrained diffusion models due to extensive fine-tuning for high fidelity, making prompt controllability difficult across diverse scenarios.

To address these challenges, we propose ODTSR, a one-step diffusion model for Real-ISR based on Qwen-Image [39], that jointly ensures fidelity and controllability. ODTSR introduces a Noise-hybrid Visual Stream (NVS) design in diffusion transformer [27] (DiT) architecture: a new visual stream receives LQ with adjustable noise (Control Noise): when this noise level is minimal or even zero, a clean LQ ensures strong fidelity and the noise level can be increased as needed to enhance prompt controllability. Meanwhile, the original visual streams take in LQ images with consistent noise (Prior Noise) to inherit denoising capability from the pretrained diffusion model. For further efficiency and controllability, ODTSR adopts a Fidelity-aware Adversarial Training (FAA) strategy: fine-tuning pretrained DiT as the discriminator, adversarial signals are dynamically adjusted based on the level of Control Noise to enhance controllability and achieve one-step inference.

As shown in Tab. 1, compared with current state-of-the-art (SOTA) methods, our proposed ODTSR jointly ensures fidelity and bilingual prompt controllability in a single-step manner. As a one-step method, ODTSR not only supports aiming at fidelity like other one-step SOTA methods PiSA-SR [32] and TSD-SR [7], but also enables prompt controllability like multi-step SOTA methods SUPIR [46] and DiT4SR [8]. The proposed ODTSR outperforms all these methods in offering superior quality and greater flexibility as demonstrated by extensive experiments. ODTSR also shows strong generalization to cross-domain and long-tail scenarios; for instance, it achieves readable and style-consistent restoration of complex Chinese textual images without training on specific dataset, substantially reducing annotation and adaptation costs in practice.

To summarize, we make the following contributions:

- We introduce ODTSR, a one-step diffusion model for Real-ISR based on Qwen-Image [39]. To the best

of our knowledge, this is the first one-step Real-ISR model with over 20B parameters that support prompts in both English and Chinese.

- We propose a Noise-hybrid Visual Stream (NVS) design, introducing a Control Noise stream for achieving fidelity and controllability simultaneously, while inheriting denoising capability from the pretrained diffusion model by denoising at Prior Noise stream.
- We propose a Fidelity-aware Adversarial Training (FAA) paradigm adjusting adversarial signals dynamically to reinforce controllability and achieving one-step inference to sidestep the computational burden of multi-step sampling from a large diffusion model.
- Our proposed ODTSR achieves superior performance on generic Real-ISR datasets and supports flexible, bilingual prompt controllability, while covering challenging sub-domains such as Chinese text images, fine-grained texture and face images in the scene without specialty training as shown in Fig. 1.

2. Related Work

Diffusion-based Real-ISR. The success of large-scale text-to-image (T2I) diffusion models such as Stable Diffusion (SD) [9, 28, 29] and Flux [3, 20] inspires researchers to leverage these pretrained models to address Real-ISR. StableSR [34] incorporates LQs into UNet-based SD via trainable time-aware encoder. DiffBIR [24] utilizes a ControlNet-like [47] reconstruction module. SeeSR [41] introduces degradation tags to guide the diffusion process. PASD [43] incorporates high-level semantic guidance to the diffusion model. OSEDiff [40] introduces VSD Loss [37, 45] to achieve one-step inference. PiSA-SR [32] proposes a dual-lora approach, considering pixel-level and semantic-level enhancement. TVT [44] trains a 4× VAE [17] module for SD to achieves better quality. Built upon SDXL [28], SUPIR [46] introduces scaling-up in diffusion-based Real-ISR. When diffusion models enter the era of DiT [27], TSD-SR [7] first introduces target score distillation to pretrained SD3 [9] model. DiT4SR [8] investigates a more effective LQ conditioning mechanism in DiT compared to ControlNet-like module. FluxSR [21] proposes flow trajectory distillation to distill a multi-step flow matching model into one-step. However, all the methods mentioned above cannot simultaneously achieve both fidelity and prompt controllability in a one-step manner, which leaves room for further exploration.

3. Motivation

In this section, we begin with an intuitive analysis of the Qwen-Image [39], a leading-edge T2I model which demonstrates significant advances in text rendering and further supports prompts in both English and Chinese, demonstrat-

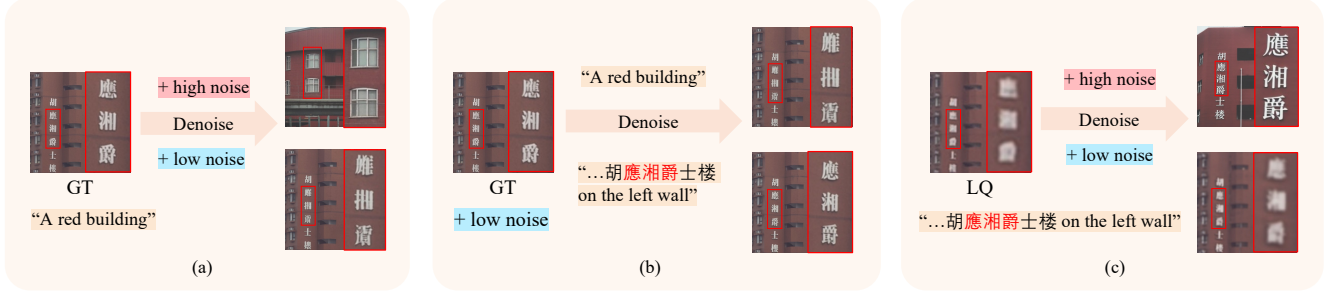


Figure 2. **Effects of Noise on Fidelity and Controllability.** Based on pretrained Qwen-Image, (a) shows the denoising results of ground-truth (GT) under the same prompt and different levels of noise. (b) adopts low noise level and different prompts (with Chinese annotation). (c) studies the effects of noise on LQ with the same prompt. High-noise inputs improve perceptual quality and controllability but reduce fidelity, whereas low-noise inputs preserve original details yet fail to deliver enhanced super-resolution effects.

ing that such a model can inherently process images in a prompt-guided manner while achieving fidelity and controllability simultaneously through modifying the noise interpolation with the input image. However, LQs cannot be restored inherently only through this process, inspiring the proposed Noise-hybrid Visual Stream design.

3.1. Preliminary

Let $x_0 \sim p_{\text{data}}$ denote a sample from the real data distribution, and let $x_1 \sim \mathcal{N}(0, I)$ be a sample from a simple prior (e.g. Gaussian noise). Flow matching models define a continuous-time trajectory x_t between x_1 and x_0 , and learn a vector field $v_\theta(x, t)$ to match the data flow. According to Rectified Flow [25], the intermediate latent variable x_t at timestep t and its corresponding velocity v_t can be calculated as:

$$x_t = tx_1 + (1-t)x_0, \quad v_t = \frac{dx_t}{dt} = x_1 - x_0, \quad (1)$$

where $t \in [0, 1]$. During training, the model minimizes the mean squared error loss:

$$\mathcal{L}(\theta) = \mathbb{E}_{(x_0, c) \sim \mathcal{D}} \|v_\theta(x_t, t, c) - v_t\|^2, \quad (2)$$

where $v_\theta(x_t, t, c)$ is the velocity predicted by the model, c denotes the text prompt, and \mathcal{D} denotes the training dataset.

3.2. Effects of Noise on Fidelity and Controllability

In this section, we analyze the performance of Qwen-Image [39] when directly applied to Real-ISR tasks through noise addition and denoising, especially considering the fidelity and prompt controllability.

At intermediate timesteps during inference, the model naturally performs a dual-conditioned task: it predicts the velocity $v_\theta(x_t, t, c)$ based on the noised latent x_t and text prompt c . The inherent conditioning mechanism on partially noised inputs and prompt guidance enables controlled image manipulation. To investigate its applicability to Real-ISR, we begin by conducting a controlled experiment on

a ground-truth (GT) high-resolution image x_{GT} , before extending the analysis to low-quality inputs. Specifically, we select two different timesteps $t_s \in \{0.90, 0.29\}$ as the starting points and construct corresponding noisy intermediates x_{t_s} by linearly interpolate the clean image x_{GT} and the noise $\epsilon \sim \mathcal{N}(0, I)$. According to Eq. (1), the initialization at timestep t is given by :

$$x_{t_s} = (1 - t_s)x_{\text{GT}} + t_s\epsilon, \quad \epsilon \sim \mathcal{N}(0, I), \quad (3)$$

where larger t_s values indicate stronger noise corruption and smaller t_s values retain more information from the original image x_{GT} . Each noisy intermediate x_{t_s} is then denoised through the remaining diffusion steps, conditioned on the input prompt c .

This setup allows us to visualize how different noise levels affect the reconstruction fidelity and prompt controllability. As shown in Fig. 2(a), under strong noise level (high t values, “+high noise”), although most of the original structures are corrupted (e.g. Chinese characters turn into windows), the diffusion model is still able to recover semantic structures guided by the prompt, while maintaining a certain degree of low-level consistency and an acceptable image quality. Meanwhile, under light noise level (low t values, “+low noise”), most of the structure is retained, while fine-grained structure like Chinese characters are corrupted. Then we further introduce specific text prompt as shown in Fig. 2(b). Under light noise level, text prompt still works surprisingly as it fixes the corrupted Chinese characters while retaining the other original structures.

We then replace the clean ground-truth sample x_{GT} with a low-quality image x_{LQ} . The corresponding noisy intermediate is then constructed as:

$$x_{t_s} = (1 - t_s)x_{\text{LQ}} + t_s\epsilon, \quad \epsilon \sim \mathcal{N}(0, I). \quad (4)$$

As shown in Fig. 2(c), under strong noise level, although the diffusion model is able to significantly improve image quality and reconstruct Chinese characters guided by the prompt, low-level fidelity is unacceptably corrupted. Under

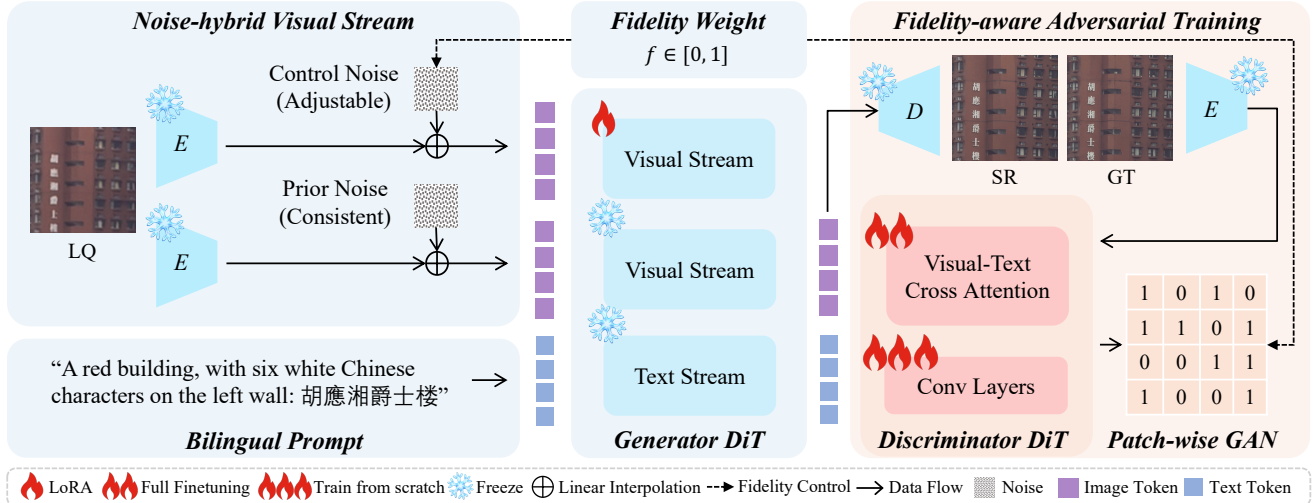


Figure 3. **Overall framework.** We extend the visual stream into a frozen *Prior Noise* stream that preserves the pretrained diffusion prior and a *Control Noise* stream that adaptively modulates noise based on the *Fidelity Weight* to restore fine details, forming a *Noise-hybrid Visual Stream*. Leveraging the *Fidelity Weight* to adjust adversarial signals adaptively, *Fidelity-aware Adversarial Training* enhances controllability and achieves one-step inference.

light noise level, the image quality remains low, although the fine-grained structures (Chinese characters) are slightly clearer compared with LQ.

In a nutshell, regardless of the quality of the input image, a higher noise level leads to stronger prompt controllability and higher quality, and low noise level maintains low-level fidelity while still having prompt-guided fine-grained control. This comes very close to ensuring both fidelity and prompt controllability in Real-ISR, and most importantly, it is the capability that the pretrained model possesses out-of-the-box without requiring any training. This inspires us to make optimal adaptations to the pretrained DiT model based on denoising capability tailored to varying noise levels. We thus propose the Noise-hybrid Visual Stream design.

4. Method

In this section, we first formulate the SR task as a one-step denoising process, then introduce the Noise-hybrid Visual Stream (NVS) for achieving fidelity and prompt controllability simultaneously. To further enhance controllability, a Fidelity-aware Adversarial Training (FAA) scheme is proposed. Finally, we describe the training objectives of the generator and discriminator under adversarial training. The whole framework is shown in Fig. 3.

4.1. Model Formulation

Let E and D denote the encoder and decoder of the pretrained variational auto-encoder (VAE), which map images to and from the latent space z . We denote by I_{LQ} and I_{GT} the low-quality and ground-truth RGB images, respectively,

and by $x_{LQ} = E(I_{LQ})$ and $x_{GT} = E(I_{GT})$ their corresponding latent representations. Our goal is to obtain the restored image $I_{SR} = D(x_{pred})$ from the predicted latent feature x_{pred} .

The Diffusion Transformer (DiT) architecture [27] is a widely adopted backbone, featuring a simpler structure than UNet and better scalability. Building upon DiT, MMDiT [9] proposes an effective strategy for multi-modal information fusion by retaining modality-specific linear projections for computing Q, K, and V, while restricting cross-modal interaction to attention operator.

The base model we employ, Qwen-Image [39], also adopts a similar double-stream design, consisting of a visual and a textual stream.

4.2. Noise-hybrid Visual Stream

From the observations in Sec. 3.2, directly applying a noised LQ latent to the pretrained visual stream presents a trade-off: high-noise inputs improve perceptual quality but reduce fidelity, whereas low-noise inputs preserve original details yet fail to deliver enhanced super-resolution effects. To address this issue, we extend the original visual stream into two branches: a **Prior Noise** stream and a **Control Noise** stream.

The Prior Noise stream injects a fixed level of noise to x_{LQ} , denoted by a hyperparameter t_p , following Eq. (1):

$$x_{t_p} = (1 - t_p)x_{LQ} + t_p\epsilon, \quad \epsilon \sim \mathcal{N}(0, I). \quad (5)$$

This stream remains frozen to preserve the pretrained diffusion prior as much as possible.

Table 2. **Real-ISR**: Quantitative comparisons on *RealSR*, *DRealSR*, and *DIV2K-Val*. The best and the second-best are highlighted in **bold** and underline. ‘‘CFG’’ denotes ‘‘classifier free guidance scale’’ in multi-step methods, and ‘‘f’’ denotes ‘‘fidelity weight’’ in ODTSR.

Dataset	Method	Step(s)	LPIPS↓	DISTS↓	MUSIQ↑	MANIQA↑	FID↓	PSNR↑	SSIM↑
RealSR	OSDiff	1	0.2921	0.2128	69.09	0.6326	123.49	25.15	0.7341
	PiSA-SR	1	0.2672	<u>0.2044</u>	<u>70.15</u>	0.6560	124.09	<u>25.50</u>	<u>0.7417</u>
	TSD-SR	1	0.2743	0.2104	71.19	0.6347	114.45	24.81	0.7172
	TVT	1	<u>0.2597</u>	0.2061	69.89	0.6232	<u>109.90</u>	25.81	0.7596
	SUPIR (CFG=4.0)	50	0.3541	0.2488	62.09	0.5780	130.38	23.65	0.6620
	DiT4SR (CFG=8.0)	40	0.3215	0.2251	67.76	<u>0.6564</u>	118.55	23.50	0.6657
	ODTSR (f=1.0, w/o prompt)	1	0.2398	0.1894	68.29	0.6622	101.49	25.07	0.7361
DRealSR	OSDiff	1	0.2968	0.2165	64.65	0.5895	135.29	27.92	<u>0.7835</u>
	PiSA-SR	1	0.2960	0.2169	<u>66.11</u>	0.6146	<u>130.48</u>	28.32	0.7804
	TSD-SR	1	0.2966	<u>0.2136</u>	66.61	0.5850	135.32	27.77	0.7559
	TVT	1	<u>0.2899</u>	0.2205	65.56	0.5776	134.28	<u>28.27</u>	0.7899
	SUPIR (CFG=4.0)	50	0.4243	0.2795	58.79	0.5471	169.48	25.09	0.6460
	DiT4SR (CFG=8.0)	40	0.3869	0.2508	65.75	0.6287	163.05	25.40	0.6657
	ODTSR (f=1.0, w/o prompt)	1	0.2592	0.1926	62.86	<u>0.6227</u>	119.86	28.14	0.7736
DIV2K-Val	OSDiff	1	0.2942	0.1975	67.96	0.6147	26.34	23.72	<u>0.6109</u>
	PiSA-SR	1	0.2823	0.1934	<u>69.68</u>	0.6401	25.09	23.87	0.6058
	TSD-SR	1	0.2673	<u>0.1821</u>	71.69	0.6226	<u>23.29</u>	23.02	0.5808
	TVT	1	0.2773	0.1860	68.67	0.6060	24.78	24.23	0.6292
	SUPIR (CFG=4.0)	50	0.3919	0.2312	63.86	0.5903	31.40	22.13	0.5259
	DiT4SR (CFG=8.0)	40	0.3448	0.2100	68.07	<u>0.6430</u>	30.57	21.78	0.5485
	ODTSR (f=1.0, w/o prompt)	1	<u>0.2761</u>	0.1700	67.94	0.6438	21.47	<u>23.92</u>	0.6108

The Control Noise stream, in contrast, dynamically modulates the noise level according to a user-controllable **Fidelity Weight** $f \in [0, 1]$. When $f = 0$, the noise level t_c matches t_p , whereas $f = 1$ corresponds to no added noise ($t_c = 0$). Intermediate values are linearly mapped from $[0, 1]$ to $[t_p, 0]$, yielding a fidelity controllable latent representation:

$$x_{t_c} = (1 - t_c)x_{LQ} + t_c\epsilon, \quad t_c = (1 - f) \cdot t_p. \quad (6)$$

During training, the value of f is uniformly sampled from the range $[0, 1]$, and t_p is empirically set to 0.43. The parameters of the Control Noise stream are initialized from the Prior Noise stream and finetuned via LoRA [12].

Finally, all streams are jointly attended via the multi-modal DiT to predict the velocity field that updates the noisy latent toward the high-quality target in a single step:

$$x_{\text{pred}} = x_{t_p} + (0 - t_p)v_{\theta}(x_{t_p}, x_{t_c}, t_p, c), \quad (7)$$

$$I_{\text{pred}} = D(x_{\text{pred}}), \quad (8)$$

where c denotes the text prompt. This formulation maintains alignment with the pretrained diffusion prior via the Prior Noise stream, while the Control Noise stream delivers a controllable fidelity-conditioning signal and adaptively restores high-frequency details, together constituting the generator of ODTSR.

4.3. Fidelity-aware Adversarial Training

Although we have made the input as consistent as possible with the pretrained design (i.e., using noised latent

features), converting the remaining multi-step denoising process into a single step remains a challenging training problem. Inspired by Diffusion Adversarial Post-Training (APT) [23], since our input is the noised LQ latent rather than pure noise, we skip the discrete-time consistency distillation[30, 31] stage and directly perform single-stage adversarial training under Real-ISR task.

Training objective of generator. We train the generator with the reconstruction loss \mathcal{L}_{rec} in RGB space and adversarial loss $\mathcal{L}_{\text{adv}}^G$ in latent space. We set \mathcal{L}_{rec} as the weighted sum of MSE loss and LPIPS loss:

$$\mathcal{L}_{\text{rec}} = \mathcal{L}_{\text{MSE}}(I_{\text{pred}}, I_{\text{GT}}) + \lambda_1 \mathcal{L}_{\text{LPIPS}}(I_{\text{pred}}, I_{\text{GT}}), \quad (9)$$

where λ_1 is a weighting scalar. As for \mathcal{L}_{adv} , inspired by R3GAN [13], we replace the non-saturating GAN loss[10] used in APT by a relativistic gan loss[14] to avoid the potential mode collapse problem[18]:

$$\mathcal{L}_{\text{adv}}^G = -\mathbb{E}_{x_r}[\log(1 - R(x_r, x_f))] - \mathbb{E}_{x_f}[\log(R(x_f, x_r))], \quad (10)$$

where $x_f = x_{\text{pred}}$ and $x_r = x_{\text{GT}}$. $R()$ is formulated as:

$$R(x_r, x_f) = \sigma(D(x_r, t, c) - D(x_f, t, c)), \quad (11)$$

where σ is the sigmoid function, t is the timestep for DiT based discriminator, c denotes the text prompt and D is the non-transformed patchified discriminator output.

Fidelity-aware Formulation Conventional adversarial super-resolution methods typically train the generator with

Table 3. **Controllable Real-ISR**: Quantitative comparisons on *RealSR* and *RealCE-Val*. The best and the second-best are highlighted in **bold** and underline. “*” suggests TVT is the only method trained on *RealCE* training set.

Dataset	Method	LPIPS↓	DISTS↓	MUSIQ↑	MANIQA↑	FID↓	CLIP-T↑	NED↑	PSNR↑	SSIM↑
RealSR (w/ prompt by default)	SUPIR (CFG=4.0)	0.3708	0.2459	61.52	0.5960	117.02	33.97	-	24.82	0.6647
	SUPIR (CFG=1.0)	0.4113	0.2808	55.84	0.5262	125.13	30.66	-	25.66	0.6501
	DiT4SR (CFG=8.0)	0.3315	0.2244	67.36	0.6612	121.73	33.49	-	23.18	0.6493
	DiT4SR (CFG=1.0)	0.2715	0.1963	61.94	0.6047	110.25	31.57	-	24.90	0.7254
	ODTSR (f=0.2)	0.3212	0.2211	69.11	0.6824	112.10	34.56	-	21.70	0.6146
	ODTSR (f=1.0)	0.2310	0.1815	68.22	<u>0.6680</u>	91.12	<u>34.01</u>	-	<u>25.09</u>	0.7382
	ODTSR (f=1.0, w/o prompt)	<u>0.2398</u>	<u>0.1894</u>	<u>68.29</u>	0.6622	<u>101.49</u>	32.37	-	25.07	<u>0.7361</u>
RealCE-val (w/o prompt by default)	OSDiff	0.2967	0.2277	64.83	0.5863	86.21	-	0.6927	18.36	0.6800
	PiSA-SR	0.2825	0.2277	64.83	0.6090	82.58	-	0.7137	<u>19.48</u>	0.6923
	TSD-SR	0.2940	0.2396	66.98	0.6057	86.22	-	0.7205	19.00	0.6625
	TVT*	0.2935	0.2348	66.50	0.5980	83.85	-	0.7179	19.27	0.6898
	SUPIR (CFG=4.0)	0.4203	0.2867	51.99	0.5030	87.23	-	0.6877	19.58	0.5784
	DiT4SR (CFG=8.0)	0.3721	0.2662	66.09	0.6443	95.90	-	0.6794	17.66	0.6013
	ODTSR (f=1.0)	0.2843	<u>0.2114</u>	66.52	<u>0.6523</u>	<u>70.05</u>	-	<u>0.7609</u>	18.78	0.6863
	ODTSR (f=1.0, w/ prompt)	<u>0.2830</u>	0.2097	<u>66.78</u>	0.6565	68.05	-	0.8475	18.75	<u>0.6891</u>

a fixed combination of reconstruction loss \mathcal{L}_{rec} and adversarial loss $\mathcal{L}_{\text{adv}}^G$, regardless of the degradation of the low-quality input. However, under our fidelity-aware formulation, the latent input x_{t_c} is dynamically perturbed according to the controllable Fidelity Weight f , leading to varying information availability and distinct reconstruction difficulties. To ensure consistency with this design, we modulate the balance between \mathcal{L}_{rec} and $\mathcal{L}_{\text{adv}}^G$ by the fidelity weight f , which defines the overall generator objective:

$$\mathcal{L}_G = \mathcal{L}_{\text{rec}} + (f \lambda_{\min} + (1 - f) \lambda_{\max}) \mathcal{L}_{\text{adv}}^G, \quad (12)$$

where λ_{\min} and λ_{\max} denote the minimum and maximum weights of the adversarial loss, corresponding to high-fidelity ($f = 1$) and low-fidelity ($f = 0$) inputs, respectively. Intuitively, as the Fidelity Weight f decreases (more degraded input), the adversarial weight increases, encouraging the generator to synthesize realistic details according to prompt input; conversely, as f increases (higher-quality input), the adversarial contribution is reduced, favoring reconstruction fidelity.

Training objective of discriminator. We adopt the Wan2.1 [33] architecture as our discriminator, which leverages the same VAE encoder as Qwen-Image. Wan2.1 also builds upon the DiT backbone, in which textual conditioning is introduced through cross-attention. We initialize the discriminator with pretrained weights and fine-tune all parameters jointly. Unlike APT, we do not introduce additional cross-attention layers for producing a single scalar score. Instead, we append two 2D convolutional layers to the transformer outputs to produce patch-wise discrimination scores.

We train the discriminator with the adversarial loss $\mathcal{L}_{\text{adv}}^D$ and regularization loss \mathcal{L}_{reg} . The adversarial loss for the discriminator is formulated in a symmetrical form with respect

to the generator loss $\mathcal{L}_{\text{adv}}^G$:

$$\mathcal{L}_{\text{adv}}^D = -\mathbb{E}_{x_r}[\log(R(x_r, x_f))] - \mathbb{E}_{x_f}[\log(1 - R(x_f, x_r))]. \quad (13)$$

We also adopt the approximated R1 loss as regularization:

$$\mathcal{L}_{\text{reg}} = \|D(x_r, t, c) - D(\mathcal{N}(x_r, \sigma I), t, c)\|_2^2, \quad (14)$$

where $\mathcal{N}(x_r, \sigma I)$ denotes adding small-variance Gaussian perturbations to the real data x_r . The loss encourages the discriminator to produce similar predictions for both the original and perturbed data, effectively reducing the discriminator’s gradient on real samples. The overall training objective for the discriminator is:

$$\mathcal{L}_D = \mathcal{L}_{\text{adv}}^D + \lambda_2 \mathcal{L}_{\text{reg}}, \quad (15)$$

where λ_2 is a weighting scalar.

5. Experiments

5.1. Experimental Settings

Implementation. We train ODTSR for the $\times 4$ Real-ISR task based on Qwen-Image [39] as generator, and Wan2.1-T2V-1.3B [33] as discriminator. The training process takes 10,000 iterations on 8 NVIDIA H20 GPUs with a batch size of 32. $\lambda_1 = 1.0$ in Eq. (9). $\lambda_{\min} = 0.02$, $\lambda_{\max} = 0.1$ in Eq. (12). $\lambda_2 = 5.0$ in Eq. (15). Other details are shown in the **supplementary materials**.

Datasets. For training, We utilize LSDIR [22] and FFHQ [15], where LQs are synthesized online following common degradation pipeline proposed in RealESRGAN [35]. For Real-ISR evaluation, we adopt two real-world datasets: RealSR [4] and DRealSR [38], and a synthetic dataset DIV2K-Val [1] following OSDiff [40]. In this scenario, our model’s input prompt is left empty

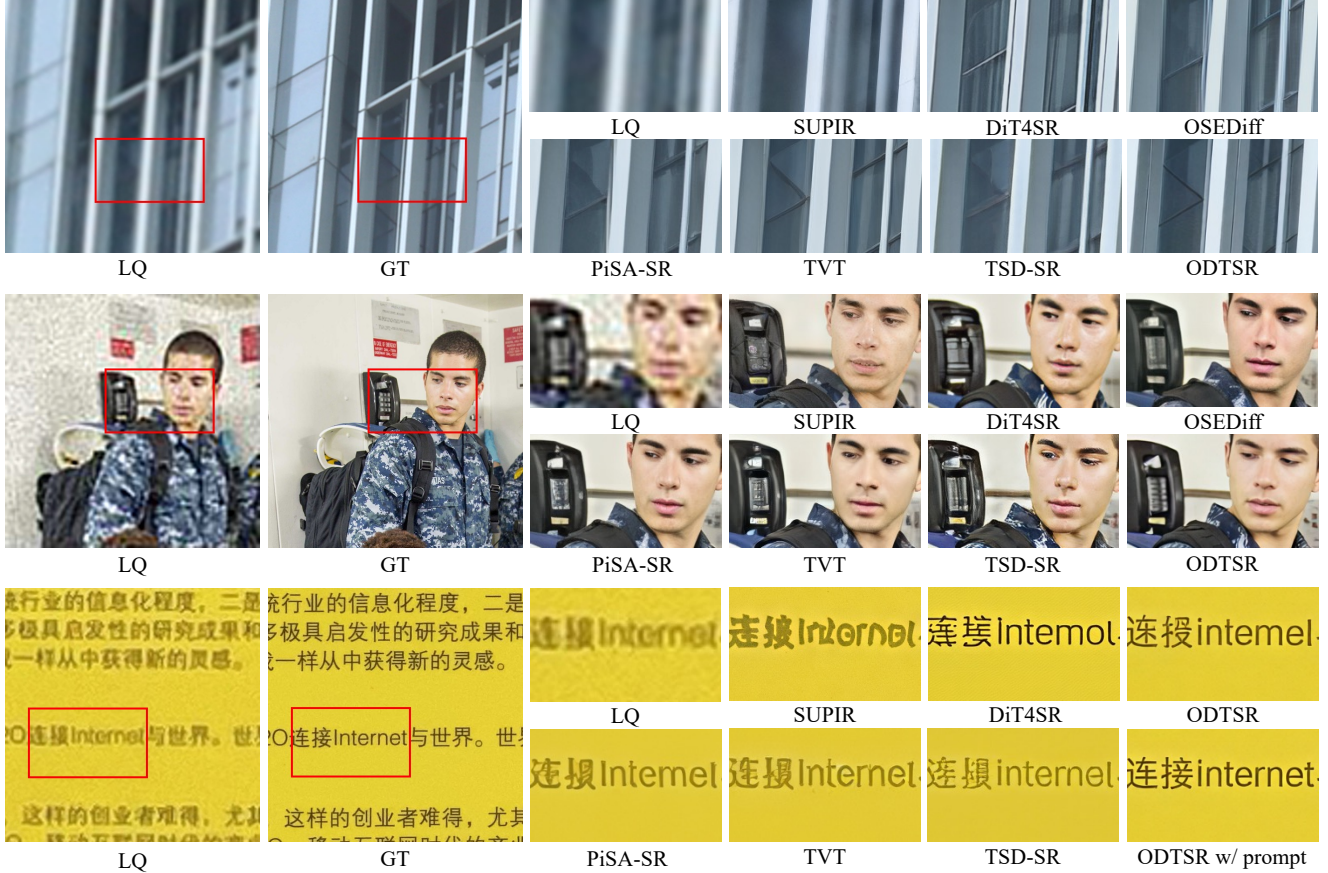


Figure 4. **Real-ISR**: Qualitative comparison on texture (1st row), face image (2nd row) and text image (3rd row). ODTSR demonstrates superior performance in these challenging cases. More results are shown in the **supplementary materials**.

and other methods retain their default settings. For controllable Real-ISR evaluation, we adopt RealSR and a scene text image super-resolution (STISR) dataset RealCE’s [26] validation set (RealCE-val). Prompts of RealSR are extract from GT using Qwen2.5-VL-7B-Instruct [2] and all methods adopt the same prompts. For RealCE-val, we center-crop all images to 512×512 and use Paddle-OCR [5] to extract text as prompt. Notably, since ODTSR is the only method capable of processing Chinese prompts, we present results with and without prompts for comprehensive comparison. More details are in the **supplementary materials**.

Metrics. Both full-reference (FR) and no-reference (NR) metrics are employed for evaluation. FR metrics include pixel-level metrics PSNR and SSIM [36], perceptual-level metrics LPIPS [48] and DISTS [6] and distribution-level FID [11]. Besides, we adopt CLIP Score (CLIP-T) to measure prompt adherence in controllable Real-ISR using jina-clip-v2 [19]. NR image quality metrics include IQA methods MUSIQ [16] and MANIQA [42]. For STISR dataset RealCE-val, we additionally employ NED (normalized edit distance) [26] to evaluate the text similarity between ground-

truth (GT) and restored image (HR):

$$NED(P, G) = 1 - \frac{ED(P, G)}{\max(|P|, |G|)}, \quad (16)$$

where P and G denote text sequences extracted from HR and GT respectively, $ED(\cdot)$ denotes edit distance between two text sequences and $|\cdot|$ denotes the length of the text.

Compared Methods. We compare ODTSR with SOTA diffusion-based one-step methods OSediff [40], PiSA-SR [32], TSD-SR [7] and TVT [44], and multi-step methods SUPIR [46] and DiT4SR [8]. We obtain all results using their official open-source codes and models under their default settings unless otherwise specified.

5.2. Comparison with State-of-the-Arts

Quantitative Comparisons of Real-ISR Tab. 2 compares the performance of our proposed ODTSR with other SOTA diffusion-based methods on three Real-ISR datasets. In general, ODTSR achieves superior results across perceptual and distribution fidelity metrics in terms of LPIPS,

DISTS and FID, while demonstrating competitive performance in NR image quality metrics like MANIQA. We also present PSNR and SSIM results for reference, demonstrating the distinction between our approach and SOTA methods, as these metrics do not adequately reflect visual fidelity and quality.

Quantitative Comparisons of Controllable Real-ISR

In prompt-guided RealSR, we conducted targeted comparisons with multi-step SOTA methods SUPIR and DiT4SR, evaluating restore quality and prompt adherence under adjustable control levels. Results are shown in Tab. 3. When aiming at fidelity (i.e. “f=1.0” in our method and low CFG scale in SUPIR and DiT4SR), ODTSR ensures leadership across all metrics including fidelity, image quality and prompt adherence, while SUPIR struggles to achieve better fidelity by adjusting CFG and DiT4SR meets a significant image quality drop in low CFG scale. When the restore target turns to prompt controllability (i.e. “f=0.2” in our method and high CFG scale in SUPIR and DiT4SR), ODTSR achieves the best prompt adherence and maintains relative high level image quality, while fidelity is reasonably reduced, which means our prompt controllability has greater and more flexible scope for adjustment.

In STISR dataset RealCE-val, ODTSR outperforms existing SOTA methods on text similarity NED by a remarkable margin even with no prompt, and with the addition of prompts, text restoration performance sees a further leap forward. It is important to emphasize that ODTSR was not trained on any specific scene text image dataset and its outstanding performance demonstrates that our proposed method effectively preserves the text rendering capability of the pretrained Qwen-Image.

Qualitative Comparisons Fig. 4 shows qualitative comparisons on Real-ISR and controllable Real-ISR. The first and second row show that ODTSR offers high quality restoration results in fine-grained textures and face images in severe degradations. Besides, the third row demonstrates ODTSR’s capability of restoring English and Chinese text image, and the quality can be further boosted with the text annotation prompt guidance (denoted as “ODTSR w/ prompt”), indicating the prompt controllability of ODTSR.

5.3. Ablation Study

Effectiveness of NVS We validate the effectiveness of ODTSR’s key design: Noise-hybrid Visual Stream (NVS), or, to elaborate, why is it necessary to introduce an additional visual stream rather than directly adjust the noise on the original visual stream. We thus train a variant, denoted as “1-visual”, which adds no additional visual stream and keeps all other training settings. Results are shown in Tab. 4. When aiming at fidelity (“f=1.0”), regardless

of whether prompt (extracted from GT) is involved, NVS shows notably better performance in fidelity, quality and prompt adherence. And in stronger prompt controllability setting (“f=0.2”), NVS sacrificing slightly lower fidelity (LPIPS and FID) for improved prompt adherence (CLIP-T) and image quality (MANIQA) means that even at the same noise level, NVS can better encourage prompt-guide generation, offering greater controllability.

Table 4. **Ablation of NVS.** We compare two variants of structure on *RealSR* dataset. The better is highlighted in **bold**. “p.” denotes “prompt”.

Structure	LPIPS↓	MANIQA↑	FID↓	CLIP-T↑
1-Visual (f=1.0, w/o p.)	0.2655	0.6387	118.08	32.01
NVS (f=1.0, w/o p.)	0.2398	0.6622	101.49	32.37
1-Visual (f=1.0, w/ p.)	0.2552	0.6499	105.94	33.94
NVS (f=1.0, w/ p.)	0.2310	0.6622	101.49	34.01
1-Visual (f=0.2, w/ p.)	0.2915	0.6688	102.03	34.35
NVS (f=0.2, w/ p.)	0.3212	0.6824	112.10	34.56

Effectiveness of FAA Tab. 5 demonstrates the effectiveness of Fidelity-aware Adversarial Training (FAA). Utilizing a fixed GAN weight, no matter low (0.02) or high (0.1), does not work well with the Control Noise stream as prompt adherence (CLIP-T) remarkably declines, since the model cannot learn to adjust the effect of prompt adaptively when Control Noise changes, and Control Noise alone corrupts the fidelity.

Table 5. **Ablation of FAA.** We compare two variants of GAN weight strategy on *RealSR* (with prompt). As fidelity weight (“f”) is reduced from 1.0 to 0.2, performance metrics showing decline are marked in **bold**.

GAN weight	FAA (f=1.0)	FAA (f=0.2)	0.02 (f=1.0)	0.02 (f=0.2)	0.1 (f=1.0)	0.1 (f=0.2)
CLIP-T	34.01	34.56↑	33.67	33.09↓	33.92	32.71↓
MANIQA	0.668	0.682↑	0.646	0.673↑	0.636	0.671↑

Ablation of Prior Noise level and other studies are also performed for a better understanding of ODTSR, which can be found in the **supplementary materials**.

5.4. User Study

To further demonstrate the performance, we conduct a user study, inviting 20 volunteers to evaluate ODTSR and other three latest SOTA methods. The results are presented in Tab. 6, demonstrating that ODTSR’s performance is more aligned with human preferences. More details can be found in the **supplementary materials**.

6. Conclusion

In this work, we propose ODTSR, a one-step DiT that achieves fidelity and controllability via novel Noise-hybrid

Table 6. **User study.** The better is highlighted in **bold**. Compared with other three SOTA methods, our model wins more than 50% votes.

Method	Ours	TSD-SR	DiT4SR	PiSA-SR
Votes	53.25%	19.4%	12.75%	14.6%

Visual Stream design and Fidelity-aware Adversarial Training strategy. We hope this work will advance the development of Real-ISR.

References

- [1] Eirikur Agustsson and Radu Timofte. Ntire 2017 challenge on single image super-resolution: Dataset and study. In *Proceedings of the IEEE conference on computer vision and pattern recognition workshops*, pages 126–135, 2017. 6, 3
- [2] Shuai Bai, Keqin Chen, Xuejing Liu, Jialin Wang, Wenbin Ge, Sibao Song, Kai Dang, Peng Wang, Shijie Wang, Jun Tang, et al. Qwen2. 5-vl technical report. *arXiv preprint arXiv:2502.13923*, 2025. 7, 2
- [3] Stephen Batifol, Andreas Blattmann, Frederic Boesel, Saksham Consul, Cyril Diagne, Tim Dockhorn, Jack English, Zion English, Patrick Esser, Sumith Kulal, et al. Flux. 1 kontext: Flow matching for in-context image generation and editing in latent space. *arXiv e-prints*, pages arXiv–2506, 2025. 2
- [4] Jianrui Cai, Hui Zeng, Hongwei Yong, Zisheng Cao, and Lei Zhang. Toward real-world single image super-resolution: A new benchmark and a new model. In *Proceedings of the IEEE/CVF international conference on computer vision*, pages 3086–3095, 2019. 6, 2, 3
- [5] Cheng Cui, Ting Sun, Manhui Lin, Tingquan Gao, Yubo Zhang, Jiaxuan Liu, Xueqing Wang, Zelun Zhang, Changda Zhou, Hongen Liu, Yue Zhang, Wenyu Lv, Kui Huang, Yichao Zhang, Jing Zhang, Jun Zhang, Yi Liu, Dianhai Yu, and Yanjun Ma. Paddleocr 3.0 technical report, 2025. 7, 2
- [6] Keyan Ding, Kede Ma, Shiqi Wang, and Eero P Simoncelli. Image quality assessment: Unifying structure and texture similarity. *IEEE transactions on pattern analysis and machine intelligence*, 44(5):2567–2581, 2020. 7
- [7] Linwei Dong, Qingnan Fan, Yihong Guo, Zhonghao Wang, Qi Zhang, Jinwei Chen, Yawei Luo, and Changqing Zou. Tsd-sr: One-step diffusion with target score distillation for real-world image super-resolution. In *Proceedings of the Computer Vision and Pattern Recognition Conference*, pages 23174–23184, 2025. 2, 7, 3
- [8] Zheng-Peng Duan, Jiawei Zhang, Xin Jin, Ziheng Zhang, Zheng Xiong, Dongqing Zou, Jimmy S Ren, Chun-Le Guo, and Chongyi Li. Dit4sr: Taming diffusion transformer for real-world image super-resolution. *arXiv preprint arXiv:2503.23580*, 2025. 2, 7, 3, 4
- [9] Patrick Esser, Sumith Kulal, Andreas Blattmann, Rahim Entezari, Jonas Müller, Harry Saini, Yam Levi, Dominik Lorenz, Axel Sauer, Frederic Boesel, et al. Scaling rectified flow transformers for high-resolution image synthesis. In *Forty-first international conference on machine learning*, 2024. 2, 4
- [10] Ian J Goodfellow, Jean Pouget-Abadie, Mehdi Mirza, Bing Xu, David Warde-Farley, Sherjil Ozair, Aaron Courville, and Yoshua Bengio. Generative adversarial nets. *Advances in neural information processing systems*, 27, 2014. 5
- [11] Martin Heusel, Hubert Ramsauer, Thomas Unterthiner, Bernhard Nessler, and Sepp Hochreiter. Gans trained by a two time-scale update rule converge to a local nash equilibrium. *Advances in neural information processing systems*, 30, 2017. 7
- [12] Edward J Hu, Yelong Shen, Phillip Wallis, Zeyuan Allen-Zhu, Yuanzhi Li, Shean Wang, Lu Wang, Weizhu Chen, et al. Lora: Low-rank adaptation of large language models. *ICLR*, 1(2):3, 2022. 5
- [13] Nick Huang, Aaron Gokaslan, Volodymyr Kuleshov, and James Tompkin. The gan is dead; long live the gan! a modern gan baseline. *Advances in Neural Information Processing Systems*, 37:44177–44215, 2024. 5
- [14] A Jolicoeur-Martineau. The relativistic discriminator: A key element missing from standard gan. *arXiv preprint arXiv:1807.00734*, 2018. 5, 3
- [15] Tero Karras, Samuli Laine, and Timo Aila. A style-based generator architecture for generative adversarial networks. In *Proceedings of the IEEE/CVF conference on computer vision and pattern recognition*, pages 4401–4410, 2019. 6, 2
- [16] Junjie Ke, Qifei Wang, Yilin Wang, Peyman Milanfar, and Feng Yang. Musiq: Multi-scale image quality transformer. In *Proceedings of the IEEE/CVF international conference on computer vision*, pages 5148–5157, 2021. 7
- [17] Diederik P Kingma and Max Welling. Auto-encoding variational bayes. *arXiv preprint arXiv:1312.6114*, 2013. 2
- [18] Youssef Kossale, Mohammed Airaj, and Aziz Darouichi. Mode collapse in generative adversarial networks: An overview. In *2022 8th International Conference on Optimization and Applications (ICOA)*, pages 1–6. IEEE, 2022. 5
- [19] Andreas Koukounas, Georgios Mastrapas, Sedigheh Eslami, Bo Wang, Mohammad Kalim Akram, Michael Günther, Isabelle Mohr, Saba Sturua, Nan Wang, and Han Xiao. jina-clip-v2: Multilingual multimodal embeddings for text and images. *arXiv preprint arXiv:2412.08802*, 2024. 7
- [20] Black Forest Labs. Flux, 2024. 2
- [21] Jianze Li, Jiezhong Cao, Yong Guo, Wenbo Li, and Yulun Zhang. One diffusion step to real-world super-resolution via flow trajectory distillation. *arXiv preprint arXiv:2502.01993*, 2025. 2
- [22] Yawei Li, Kai Zhang, Jingyun Liang, Jiezhong Cao, Ce Liu, Rui Gong, Yulun Zhang, Hao Tang, Yun Liu, Denis Demantolx, et al. Lsdir: A large scale dataset for image restoration. In *Proceedings of the IEEE/CVF Conference on Computer Vision and Pattern Recognition*, pages 1775–1787, 2023. 6, 2
- [23] Shanchuan Lin, Xin Xia, Yuxi Ren, Ceyuan Yang, Xuefeng Xiao, and Lu Jiang. Diffusion adversarial post-training for one-step video generation. *arXiv preprint arXiv:2501.08316*, 2025. 5
- [24] Xinqi Lin, Jingwen He, Ziyang Chen, Zhaoyang Lyu, Bo Dai, Fanghua Yu, Wanli Ouyang, Yu Qiao, and Chao Dong. Diff-

- bir: Towards blind image restoration with generative diffusion prior, 2024. 2
- [25] Kingchao Liu, Chengyue Gong, and Qiang Liu. Flow straight and fast: Learning to generate and transfer data with rectified flow. *arXiv preprint arXiv:2209.03003*, 2022. 3, 1
- [26] Jianqi Ma, Zhetong Liang, Wangmeng Xiang, Xi Yang, and Lei Zhang. A benchmark for chinese-english scene text image super-resolution. In *Proceedings of the IEEE/CVF International Conference on Computer Vision*, pages 19452–19461, 2023. 7, 2, 3
- [27] William Peebles and Saining Xie. Scalable diffusion models with transformers. In *Proceedings of the IEEE/CVF international conference on computer vision*, pages 4195–4205, 2023. 2, 4
- [28] Dustin Podell, Zion English, Kyle Lacey, Andreas Blattmann, Tim Dockhorn, Jonas Müller, Joe Penna, and Robin Rombach. Sdxl: Improving latent diffusion models for high-resolution image synthesis. *arXiv preprint arXiv:2307.01952*, 2023. 2
- [29] Robin Rombach, Andreas Blattmann, Dominik Lorenz, Patrick Esser, and Björn Ommer. High-resolution image synthesis with latent diffusion models. In *Proceedings of the IEEE/CVF conference on computer vision and pattern recognition*, pages 10684–10695, 2022. 2
- [30] Yang Song and Prafulla Dhariwal. Improved techniques for training consistency models. *arXiv preprint arXiv:2310.14189*, 2023. 5
- [31] Yang Song, Prafulla Dhariwal, Mark Chen, and Ilya Sutskever. Consistency models. *arXiv preprint arXiv:2303.01469*, 2023. 5
- [32] Lingchen Sun, Rongyuan Wu, Zhiyuan Ma, Shuaizheng Liu, Qiaosi Yi, and Lei Zhang. Pixel-level and semantic-level adjustable super-resolution: A dual-lora approach. In *Proceedings of the Computer Vision and Pattern Recognition Conference*, pages 2333–2343, 2025. 2, 7, 3
- [33] Team Wan, Ang Wang, Baole Ai, Bin Wen, Chaojie Mao, Chen-Wei Xie, Di Chen, Feiwu Yu, Haiming Zhao, Jianxiao Yang, et al. Wan: Open and advanced large-scale video generative models. *arXiv preprint arXiv:2503.20314*, 2025. 6
- [34] Jianyi Wang, Zongsheng Yue, Shangchen Zhou, Kelvin C.K. Chan, and Chen Change Loy. Exploiting diffusion prior for real-world image super-resolution. 2024. 2
- [35] Xintao Wang, Liangbin Xie, Chao Dong, and Ying Shan. Real-esrgan: Training real-world blind super-resolution with pure synthetic data. In *Proceedings of the IEEE/CVF international conference on computer vision*, pages 1905–1914, 2021. 1, 6, 2
- [36] Zhou Wang, Alan C Bovik, Hamid R Sheikh, and Eero P Simoncelli. Image quality assessment: from error visibility to structural similarity. *IEEE transactions on image processing*, 13(4):600–612, 2004. 7
- [37] Zhengyi Wang, Cheng Lu, Yikai Wang, Fan Bao, Chongxuan Li, Hang Su, and Jun Zhu. Prolificdreamer: High-fidelity and diverse text-to-3d generation with variational score distillation. *Advances in neural information processing systems*, 36: 8406–8441, 2023. 2
- [38] Pengxu Wei, Ziwei Xie, Hannan Lu, Zongyuan Zhan, Qixiang Ye, Wangmeng Zuo, and Liang Lin. Component divide-and-conquer for real-world image super-resolution. In *European conference on computer vision*, pages 101–117. Springer, 2020. 6, 3
- [39] Chenfei Wu, Jiahao Li, Jingren Zhou, Junyang Lin, Kaiyuan Gao, Kun Yan, Sheng-ming Yin, Shuai Bai, Xiao Xu, Yilei Chen, et al. Qwen-image technical report. *arXiv preprint arXiv:2508.02324*, 2025. 2, 3, 4, 6, 1
- [40] Rongyuan Wu, Lingchen Sun, Zhiyuan Ma, and Lei Zhang. One-step effective diffusion network for real-world image super-resolution. *Advances in Neural Information Processing Systems*, 37:92529–92553, 2024. 2, 6, 7
- [41] Rongyuan Wu, Tao Yang, Lingchen Sun, Zhengqiang Zhang, Shuai Li, and Lei Zhang. Seesr: Towards semantics-aware real-world image super-resolution. In *Proceedings of the IEEE/CVF conference on computer vision and pattern recognition*, pages 25456–25467, 2024. 2
- [42] Sidi Yang, Tianhe Wu, Shuwei Shi, Shanshan Lao, Yuan Gong, Mingdeng Cao, Jiahao Wang, and Yujiu Yang. Maniqa: Multi-dimension attention network for no-reference image quality assessment. In *Proceedings of the IEEE/CVF conference on computer vision and pattern recognition*, pages 1191–1200, 2022. 7
- [43] Tao Yang, Rongyuan Wu, Peiran Ren, Xuansong Xie, and Lei Zhang. Pixel-aware stable diffusion for realistic image super-resolution and personalized stylization. In *European conference on computer vision*, pages 74–91. Springer, 2024. 2
- [44] Qiaosi Yi, Shuai Li, Rongyuan Wu, Lingchen Sun, Yuhui Wu, and Lei Zhang. Fine-structure preserved real-world image super-resolution via transfer vae training. 2025. 2, 7
- [45] Tianwei Yin, Michaël Gharbi, Richard Zhang, Eli Shechtman, Fredo Durand, William T Freeman, and Taesung Park. One-step diffusion with distribution matching distillation. In *Proceedings of the IEEE/CVF conference on computer vision and pattern recognition*, pages 6613–6623, 2024. 2
- [46] Fanghua Yu, Jinjin Gu, Zheyuan Li, Jinfan Hu, Xiangtao Kong, Xintao Wang, Jingwen He, Yu Qiao, and Chao Dong. Scaling up to excellence: Practicing model scaling for photo-realistic image restoration in the wild. In *Proceedings of the IEEE/CVF conference on computer vision and pattern recognition*, pages 25669–25680, 2024. 2, 7, 4
- [47] Lvmin Zhang, Anyi Rao, and Maneesh Agrawala. Adding conditional control to text-to-image diffusion models. In *Proceedings of the IEEE/CVF international conference on computer vision*, pages 3836–3847, 2023. 2
- [48] Richard Zhang, Phillip Isola, Alexei A Efros, Eli Shechtman, and Oliver Wang. The unreasonable effectiveness of deep features as a perceptual metric. In *Proceedings of the IEEE conference on computer vision and pattern recognition*, pages 586–595, 2018. 7

One-Step Diffusion Transformer for Controllable Real-World Image Super-Resolution

Supplementary Material

7. Overview

In this material, we provide the following contents:

- More implementation details of ODTSR, including hyperparameters, more explanation of the Prior Noise stream, model structure and loss visualization (referring to Sec. 5.1 in the main paper);
- More details of training and testing dataset (referring to Sec. 5.1 in the main paper);
- More ablation studies related to the Prior Noise and GAN training strategies (referring to Sec. 5.3 in the main paper);
- User Study details (referring to Sec. 5.4 in the main paper);
- More qualitative comparison results of Real-ISR and controllable Real-ISR (referring to Sec 5.2 in the main paper);
- Limitation and future works (referring to Sec. 6 in the main paper)

8. Implementation Details

In this section, we present various details of the model to help readers gain a deeper understanding of its design.

8.1. Hyperparameter Overview

Table 7. A summary of the main hyperparameters used in ODTSR.

Hyperparameter	Value
Generator’s Learning Rate	constant 5e-5
Discriminator’s Learning Rate	constant 5e-6
Batch Size	32 (gradient accumulation = 4)
Generator’s Optimizer	RMSprop (alpha=0.9, momentum=0.0)
Discriminator’s Optimizer	RMSprop (alpha=0.9, momentum=0.0)
Lora Rank	128
Lora Alpha	128
Training Iters	10,000
Training Resources	8*NVIDIA H20 GPUs, within 48 hours
t_p in Eq.(5) of main paper	0.43
Fidelity Weight f	uniformly in the interval [0, 1]
λ_1 in Eq.(9) of main paper	1.0
λ_{\min} in Eq.(12) of main paper	0.02
λ_{\max} in Eq.(12) of main paper	0.1
variance σ in Eq.(14) of main paper	0.005
λ_2 in Eq.(15) of main paper	5.0
Mixed Precision Training	True (<code>float8_e4m3fn</code> and <code>bfloat16</code>)
Gradient Checkpointing	True

8.2. Explanation of t_p for Prior Noise stream

In Eq.(5) of the main paper, the hyperparameter t_p is a crucial value, as it determines the range of the noise level for LQ interpolation when the *Fidelity Weight* changes. In T2I pretrained models based on Rectified Flow [25], a **sched-**

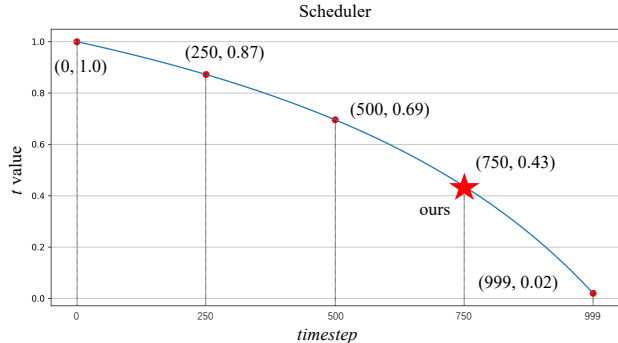


Figure 5. The **scheduler** used in Qwen-Image. The horizontal axis is the *timestep* ranging from 0 to 999, 1000 discrete timesteps in total, and the vertical axis represents the values of t . During pre-training, *timestep* is uniformly sampled to obtain t .

uler is typically used during pre-training. This scheduler establishes a relationship between *timestep* (ranging from 0 to 999, 1000 discrete timesteps in total) and t in Eq.(1) of the main paper. By sampling the timestep, the corresponding t can be obtained. The scheduler used in Qwen-Image [39] is illustrated in Fig. 5.

In our single-step training, we determine the value of t_p by deciding the timestep, which is aligned with pre-training. This is why the value 0.43 looks a bit unusual, which actually corresponds to timestep 750.

We also ablate different timestep (i.e. 250 and 500) and use their corresponding t_p values (i.e. 0.87 and 0.69) to train the model. See details in Sec. 10.1.

8.3. Model Structure Visualization

The base model we employ, Qwen-Image [39], adopts a double-stream design, consisting of a visual and a textual stream. We provide the detailed structure of a single transformer layer, as shown in Fig. 9.

8.4. Loss Curve Visualization

To help readers better understand the training dynamics, we visualize the loss curves, as shown in Fig. 6. Moreover, we summarize the common patterns observed in stable convergence as follows:

- $\mathcal{L}_{\text{MSE}}(I_{\text{pred}}, I_{\text{GT}})$: the loss decreases rapidly at the beginning and later fluctuates within a stable range.
- $\mathcal{L}_{\text{LPIPS}}(I_{\text{pred}}, I_{\text{GT}})$: shows a steady decrease (at least during the first 10k iterations).

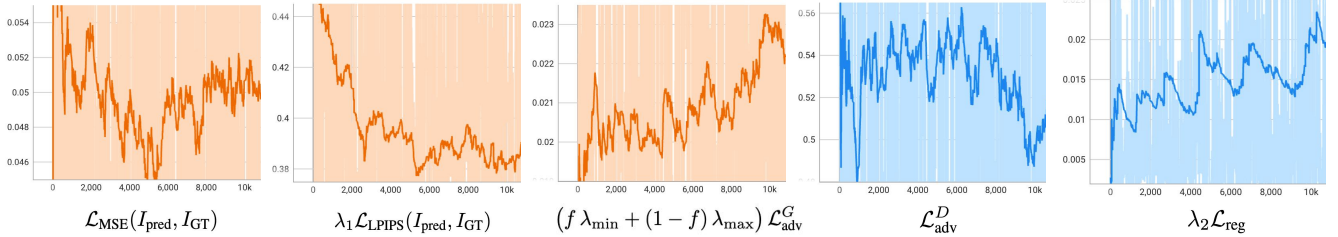


Figure 6. The visualization of the loss curves: the generator and discriminator losses are marked in different colors. Our training only needs 10,000 iterations to achieve good results. The meaning of the symbols corresponds to that in the main paper.

- \mathcal{L}_{adv}^G : shows a slight upward trend amid fluctuations.
- \mathcal{L}_{adv}^D : shows a slight downward trend amid fluctuations, and the value is less than $-\ln(\text{sigmoid}(0)) = -\ln(0.5) \approx 0.693$. This indicates that, on average, the discriminator has the ability to distinguish between real and fake samples.
- \mathcal{L}_{reg} : shows a slight upward trend amid fluctuations.

9. Dataset Details

9.1. Training Set

Like most previous methods, we use the LSDIR [22] and the first 10,000 images of FFHQ [15] as our training sets. The paired 512x512 data are constructed using the standard Real-ESRGAN [35] degradation pipeline. Specifically, the degradation hyperparameter configurations are exactly the same as those in PiSA-SR [32].

The difference is that our model requires textual descriptions during training. The discriminator always receives the description, while the generator uses the description with a probability of 0.75 and an empty description with a probability of 0.25 during each training iter. We design a set of six prompt templates to extract textual descriptions from GT images using Qwen2.5-VL-7B-Instruct [2]. These templates cover different levels of granularity, ranging from short tags to detailed captions and quality assessments:

- "Use a few word tags to summarize the main content of this image."
- "Describe the main content of this image in one sentence."
- "Describe the content of this image in a few sentences."
- "Describe possible detailed features in this image, such as text or faces; if no such targets exist, describe other details; if multiple targets exist, describe them separately."
- "Describe the quality of this image and evaluate it based on factors such as clarity, color, noise, lighting, and focal length/lens effects."
- "Describe the artistic style or form of this image (e.g., photography, illustration, painting, CG) and explain the overall tone and mood."

Since the base model we use supports both English and Chinese, we include six additional Chinese templates, each

corresponding to one of the English templates. During each training iteration, we randomly select one prompt from the total of 12 templates.

9.2. Testing Set

Controllable Real-ISR: RealSR We utilize the RealSR [4] dataset to evaluate the performance on general controllable image restoration. The difference from a standard Real-ISR task is that we provide the model with a text description. The textual descriptions for RealSR are extracted from the ground truth images using Qwen2.5-VL-7B-Instruct [2], and all methods use the same descriptions. The prompt used to extract the description is: "Describe the content of this image in a few sentences."

Controllable Real-ISR: RealCE We utilize the RealCEval [26] dataset to evaluate the performance on scene text image restoration, especially with text annotations. We center-crop all images to 512x512 and manually remove pairs where LQ and GT are not aligned. Finally, we get 260 LQ-GT pairs. For text annotations, we employ *PP-OCRv5* of Paddle-OCR [5] to extract text from GT and use it directly as the corresponding prompt.

10. More Ablation Studies

10.1. Selection of timestep in the Prior Noise stream

In this section, we investigate the impact of different *timestep* selections of Prior Noise. We train another two models with different timestep (i.e. 250 and 500) for the same training steps and compare their performance. As shown in Tab. 8, as timestep decreases from 750 to 250, which means t_p and the level of the Prior Noise increases, the reconstruction fidelity is severely compromised. This is because our Fidelity-Aware Adversarial Training strategy samples GAN weight based on t_p , and higher t_p value requires more training for fidelity (i.e. f approaches 1 in Eq.(6) and Eq.(12) of the main paper). We thus choose timestep 750 empirically.

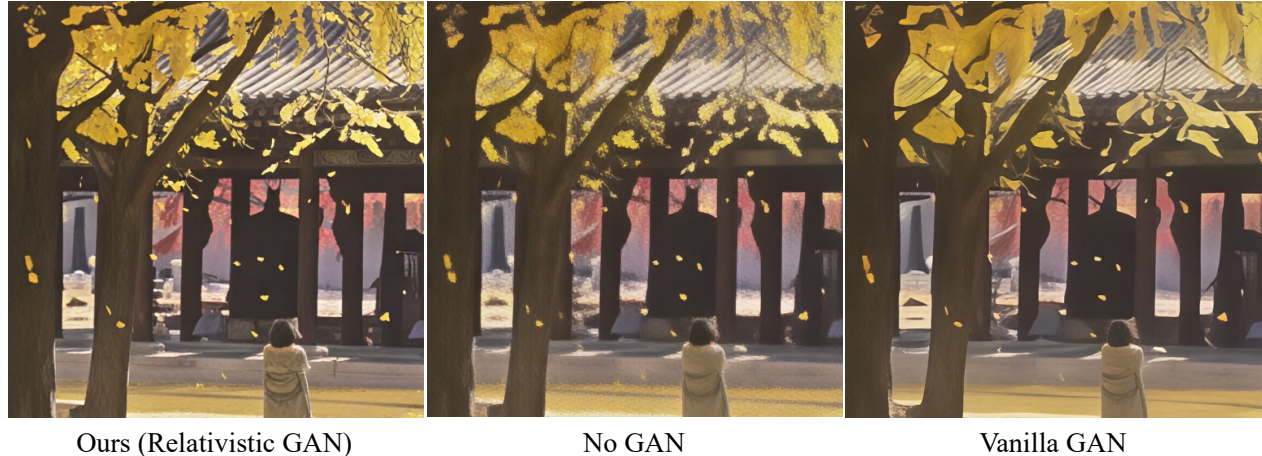


Figure 7. Visualization of GAN ablation. Trained with no GAN, model generates grid-like and blur artifacts. Trained with Vanilla GAN rather than Relativistic GAN, the restored image lacks detail and has been smoothed out.

Table 8. **Ablation of timestep of Prior Noise.** We train two models with different timestep (i.e. 250 and 500) of Prior Noise for the same training steps and compare the performance on *RealSR* dataset. *Fidelity Weight* is set to 1.0. The best is highlighted in **bold**.

Timestep	t_p	LPIPS↓	MANIQA↑	FID↓	CLIP-T↑
250	0.87	0.3318	0.6610	144.79	29.76
500	0.69	0.3057	0.6387	118.08	31.00
750 (Ours)	0.43	0.2398	0.6622	101.49	32.37

10.2. GAN training strategies

In this section, we investigate two key questions in GAN training: (1) why GAN is necessary and (2) why relativistic GAN [14] is chosen. We train two models following these two questions and evaluate their performance quantitatively and qualitatively. As shown in Tab. 9 and Fig. 7, trained without GAN (“No GAN”) is comparable in terms of fidelity, but fails in image quality, which is also demonstrated in visualization, showing grid-like artifacts and blur; trained with vanilla GAN (“Vanilla GAN”) solves grid-like artifacts but produces over-smooth restoration results and also falls behind in the metric evaluation. Overall, relativistic GAN demonstrates the best performance. This also demonstrates that PSNR cannot accurately reflect image quality.

Table 9. **Ablation of GAN Strategies.**

GAN	LPIPS↓	MANIQA↑	FID↓	PSNR↑
No GAN	0.2600	0.6180	119.28	26.07
Vanilla GAN	0.2931	0.6451	142.93	25.60
Ours (Relativistic GAN)	0.2398	0.6622	101.49	25.07

11. User Study Details

We invite 20 volunteers to evaluate ODTSR and other three latest SOTA methods (TSD-SR [7], PiSA-SR [32]

and DiT4SR [8]) in generic Real-ISR setting. 100 LQ images are randomly chosen from four datasets (RealSR [4], DRealSR [38], Div2k-val [1], RealCE-val [26]). *Fidelity Weight* is set to 1.0 and input prompt is empty in ODTSR. In the user study, volunteers are presented with six images: LQ, GT and restoration results from four methods randomly ordered. Volunteers are asked to choose the best result according to (1) fidelity with LQ and GT (2) overall image quality. We build a simple webpage for the user study, with the interface shown in Fig. 8.

12. More Qualitative Results

12.1. Real-ISR

We present more Real-ISR results in Fig. 10 and Fig. 11, comparing our ODTSR with three state-of-the-art methods PiSA-SR [32] (one-step, based on Diffusion U-Net), TSD-SR [7] (one-step, based on Diffusion Transformer) and DiT4SR [8] (multi-step, based on Diffusion Transformer), which is identical to the settings in the user study. In generic Real-ISR setting, ODTSR achieves remarkable performance in fidelity and detail quality. For example, Row 2 of Fig. 10 shows restored sculpture image with refined and realistic facial details and Row 5 of Fig. 11 shows restored correct texture of the blanket with no prompt guidance.

12.2. Controllable Real-ISR

Text scene We present more results on RealCE-val, a scene text image super-resolution dataset. We show results of ODTSR both with and without prompt. As shown in Fig. 12, ODTSR achieves higher restoration quality than other methods without prompt. When text annotation is incorporated as a prompt, some distorted characters were corrected while also demonstrating prompt controllability.

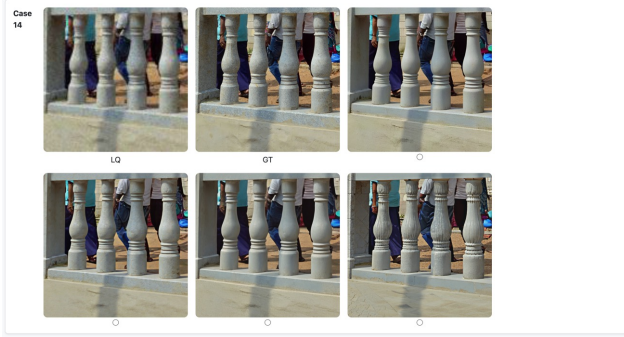


Figure 8. User Study Interface.

General scene We present more results on RealSR with prompt extracted from GT for easier visual comparison. Fig. 13 shows that ODTSR, compared with multi-step methods SUPIR [46] and DiT4SR [8], restores realistic and high-quality details under prompt control. For example, in Row 4 of Fig. 13, ODTSR restores correct details of seats and wall.

Adjustable Fidelity Weight In Fig. 14, we present results with adjustable *Fidelity Weight* (denoted as f) in ODTSR to demonstrate the scope and effectiveness of controllability. In general, as f decreases from 1 to 0, detail generation and prompt adherence gradually strengthen.

13. Limitation and Future Works

Although ODTSR achieves high fidelity and prompt controllability, its large number of parameters leads to the high computational cost. We plan to apply various model acceleration techniques to mitigate computational costs. Additionally, the *Fidelity Weight* in ODTSR is currently adjusted for the whole image, leaving room for more fine-grained control. We plan to explore more efficient and precise control approaches in the future.

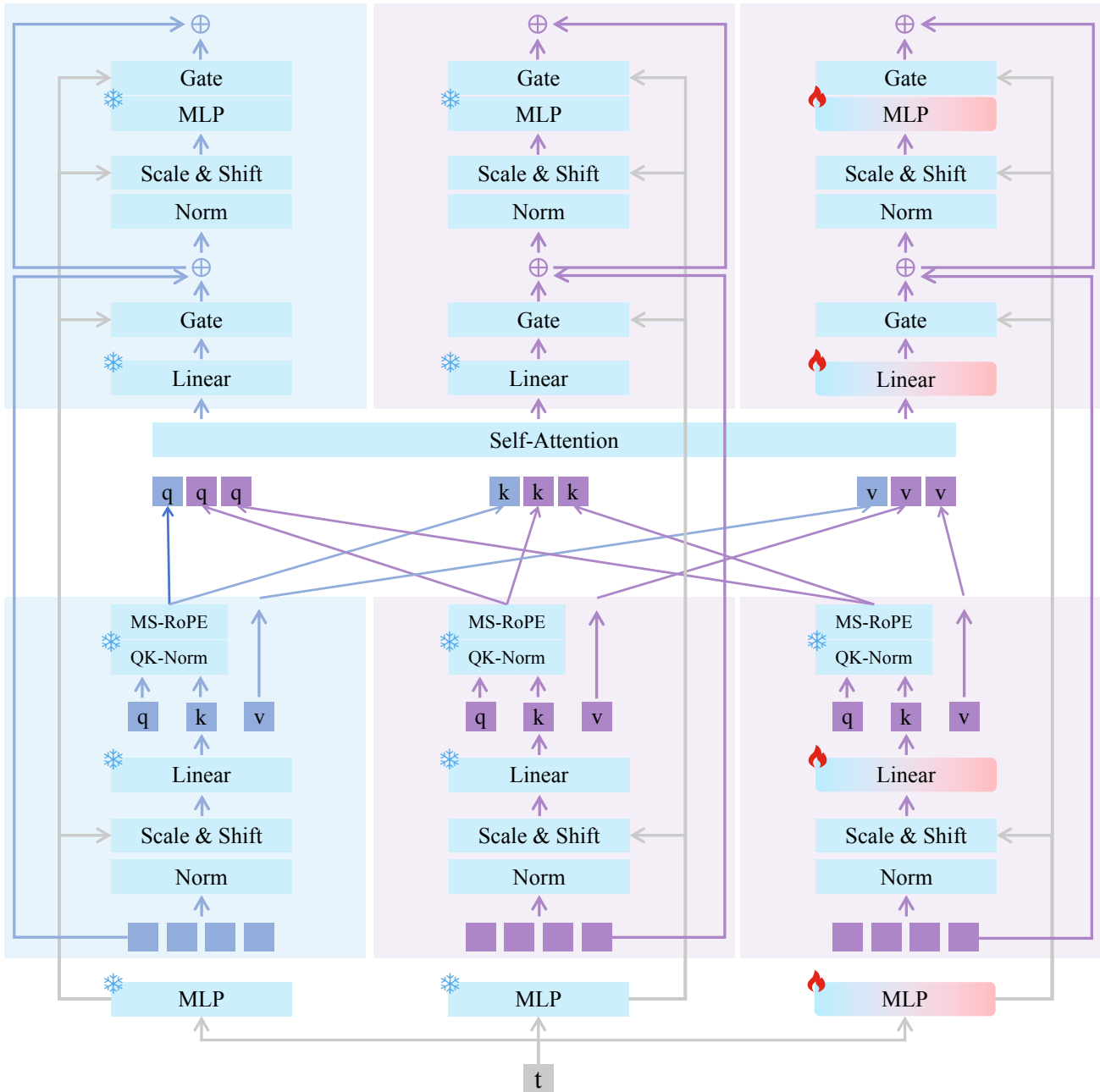


Figure 9. The model contains 60 transformer layers in total. The details of a single transformer layer are shown here: the left branch corresponds to the Text stream, the middle to the Prior Noise stream, and the right to the Control Noise stream. Among them, only the linear layers in the Control Noise stream are trained with LoRA, while all other parameters remain frozen.

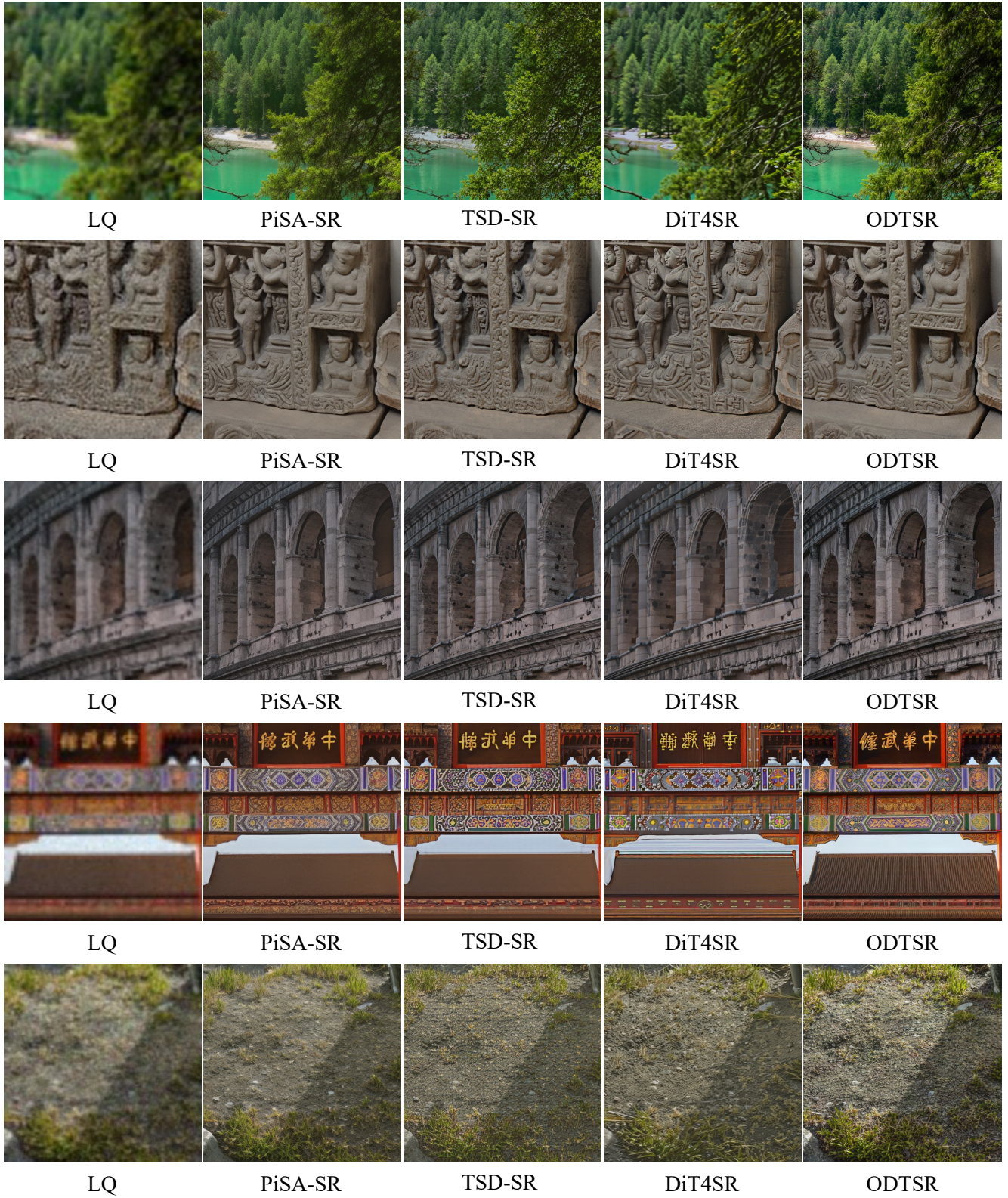


Figure 10. More qualitative results on **Real-ISR**. *Fidelity Weight* is set to 1.0 and input prompt is empty in ODTSR. ODTSR achieves remarkable performance in fidelity and detail quality.

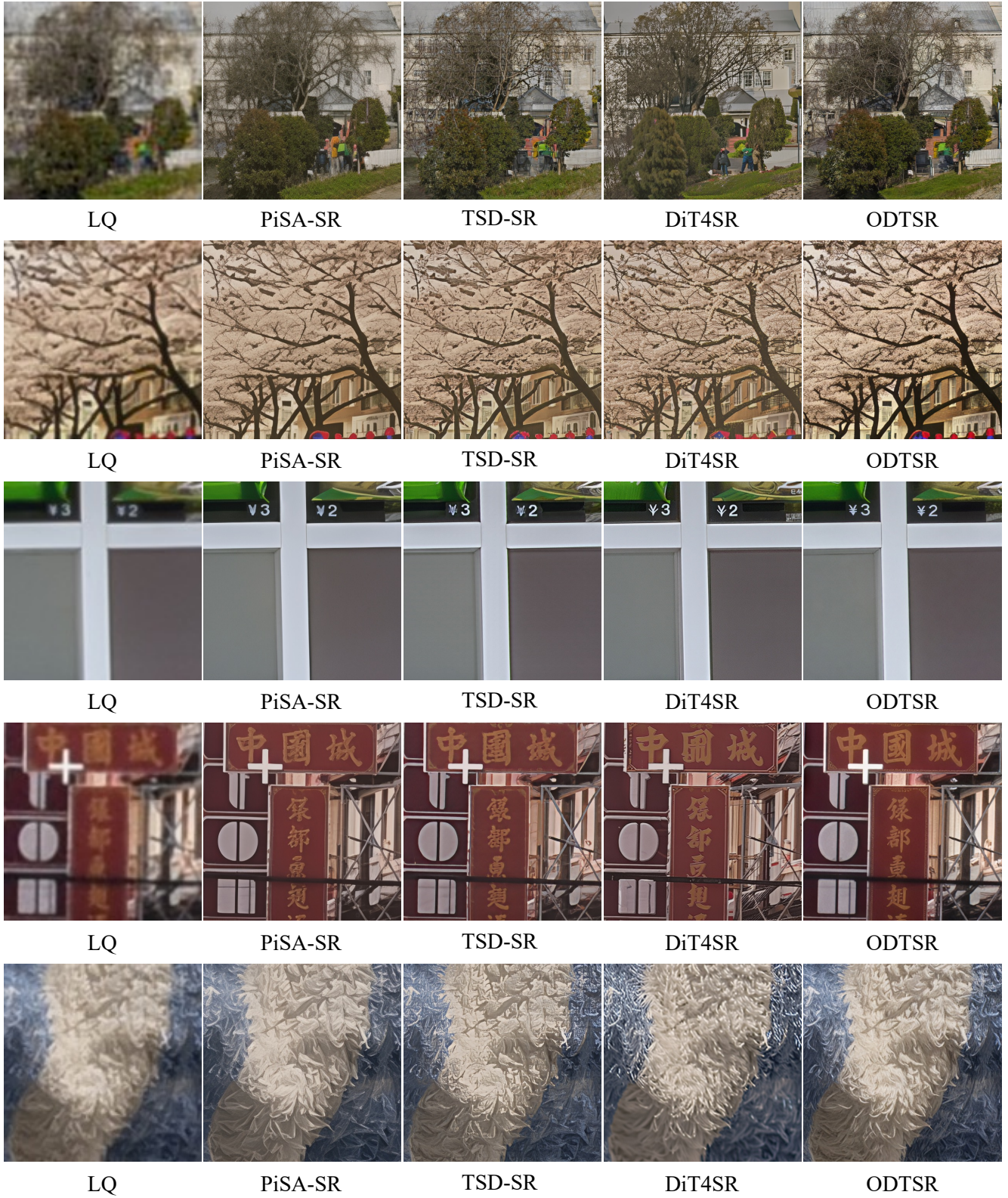


Figure 11. More qualitative results of **Real-ISR**. *Fidelity Weight* is set to 1.0 and input prompt is empty in ODTSR. ODTSR achieves remarkable performance in fidelity and detail quality.

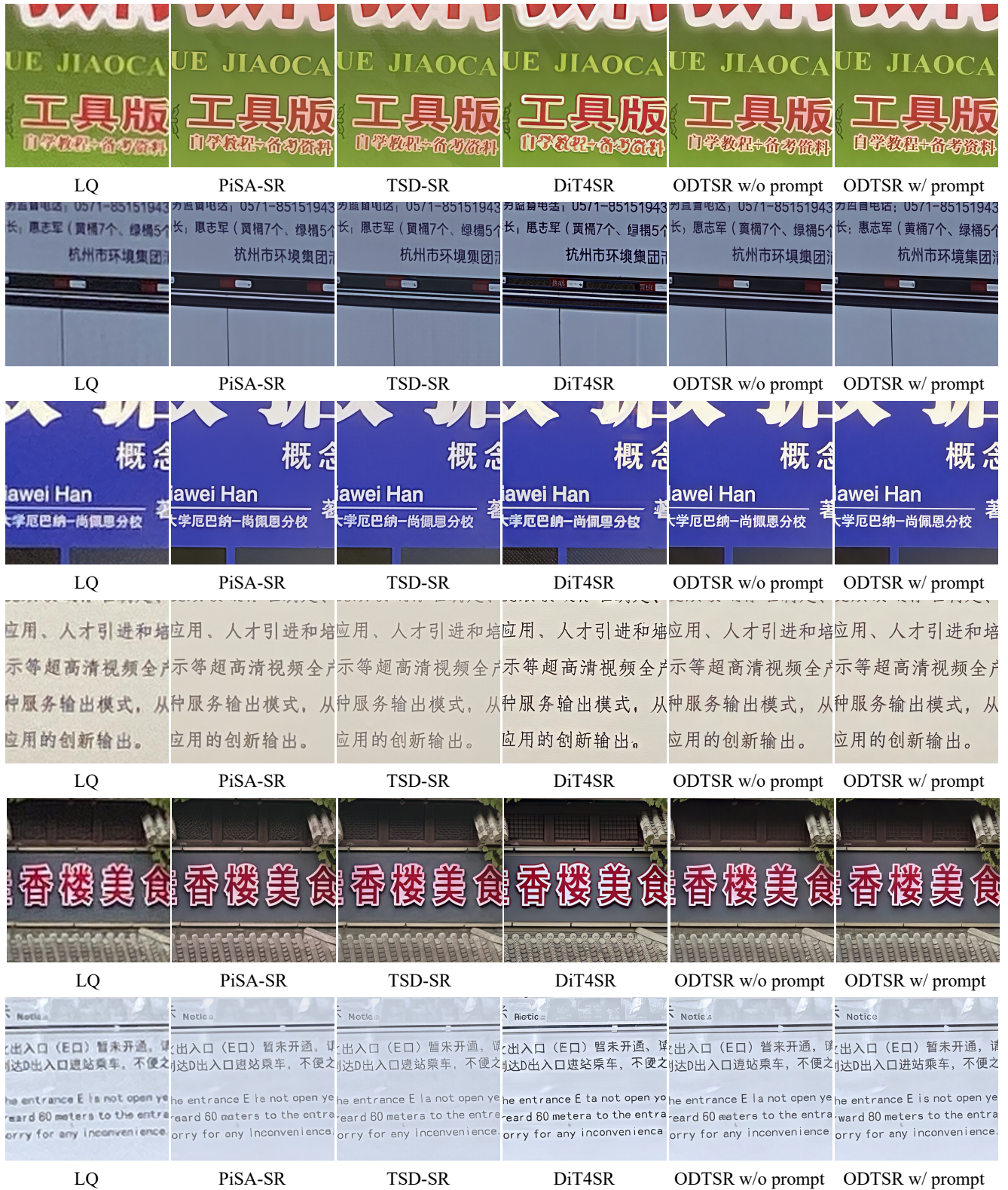


Figure 12. More qualitative results of **Controllable Real-ISR** on *RealCE-val* dataset. *Fidelity Weight* is set to 1.0 and we show results of ODTSR both with and without prompt (text annotation). ODTSR achieves higher restoration quality than other methods.

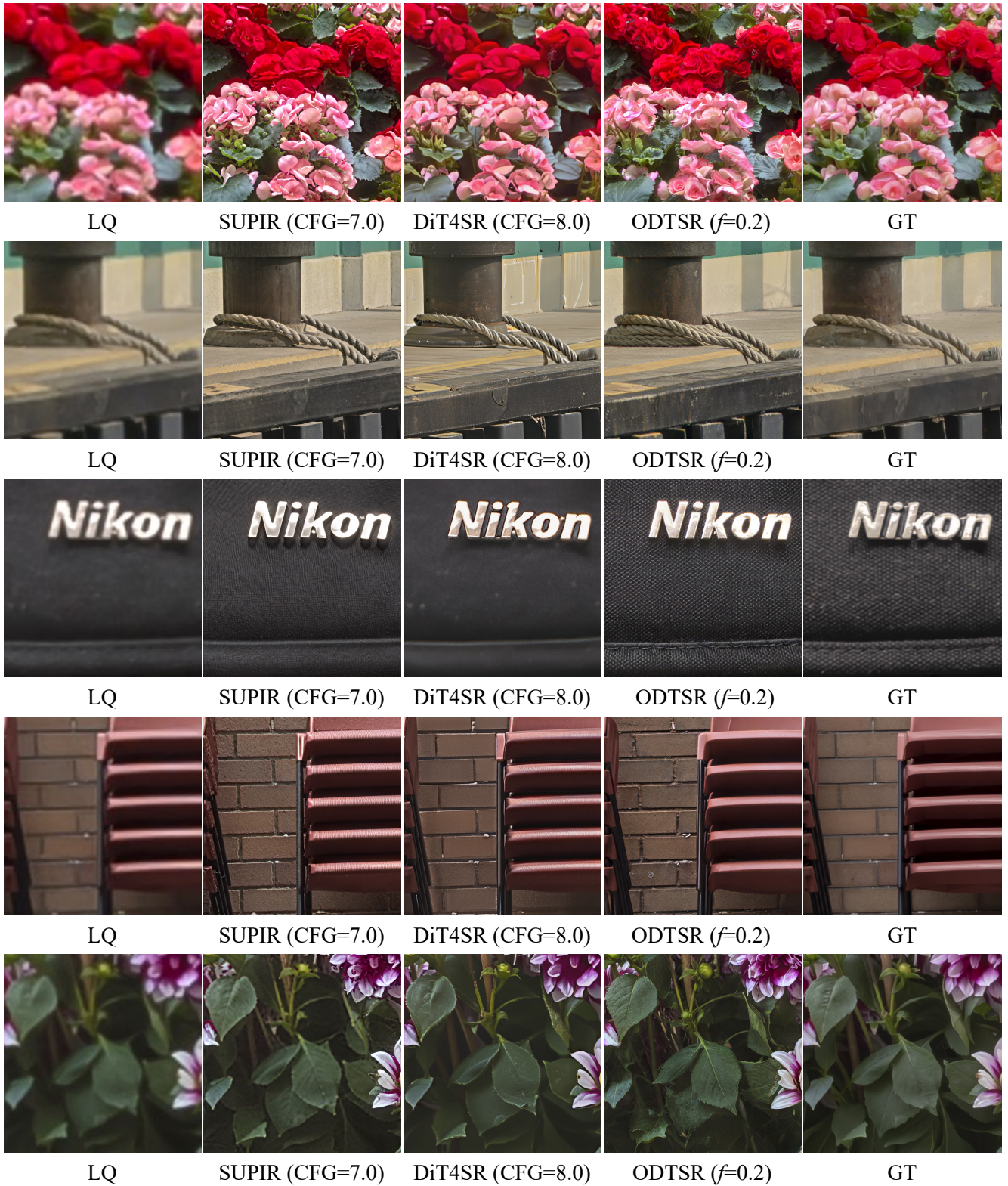


Figure 13. More qualitative results of **Controllable Real-ISR** on *RealSR* dataset. *Fidelity Weight* is denoted as f and the input prompt is extracted from GT same across three methods. ODTSR restores more realistic and higher-quality details under prompt control.

*The branches are covered with **spider webs**.*



LQ

$f=1$, w/o prompt

$f=1$, w/ prompt

$f=0.5$, w/ prompt

$f=0$, w/ prompt

***Weeds** have grown thick along the railroad tracks.*



LQ

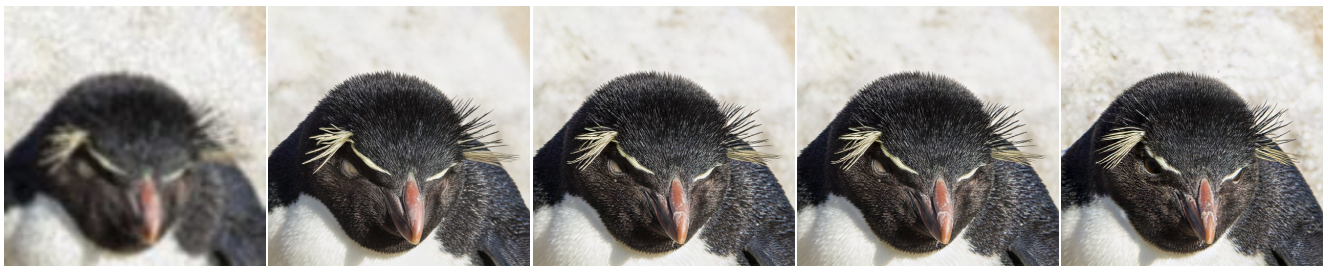
$f=1$, w/o prompt

$f=1$, w/ prompt

$f=0.5$, w/ prompt

$f=0$, w/ prompt

*The penguin watched with **wide eyes**.*



LQ

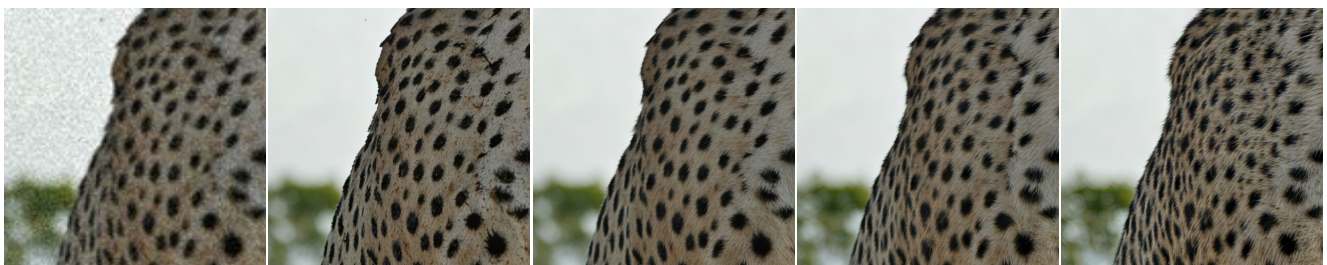
$f=1$, w/o prompt

$f=1$, w/ prompt

$f=0.5$, w/ prompt

$f=0$, w/ prompt

*The leopard's skin is covered with **fur**.*



LQ

$f=1$, w/o prompt

$f=1$, w/ prompt

$f=0.5$, w/ prompt

$f=0$, w/ prompt

Figure 14. More qualitative results of **Controllable Real-ISR** with prompt and adjustable *Fidelity Weight* (denoted as f) on *Div2k-val* dataset. As f decreases from 1 to 0, detail generation and prompt adherence gradually strengthen, demonstrating controllability of ODTSR. The prompt corresponding to the enhanced details is marked in **red**.